Reliability based fatigue assessment of existing motorway bridge

Luca D'Angelo[a,*], Alain Nussbaumer[a]

[a]*Steel structures laboratory (ICOM), Swiss Federal Institute of Technology Lausanne*

Abstract

This paper provides an original framework for the fatigue reliability analysis of a road bridge; the framework is applied to the Venoge bridge, a composite steel-concrete bridge within the A1 Swiss highway. Two critical details are selected by inspection: a longitudinal weld attachment and a cover plate welded attachment. Weigh in Motion (WIM) data from Denges station (1km far from the bridge) and a refined three-dimensional Finite Element (FE) model of the bridge are used to get realistic time-stress response at two critical locations. The fatigue failure probability of the bridge at two selected locations under the long-term effect of highway traffic is calculated for a 100 year-design life. The original contribution consists in computing the failure probability as joint probability of two events: 1) the exceeding of the constant amplitude fatigue limit (CAFL); and 2) the critical fatigue damage accumulation. The results show that fatigue is not a concern for the longitudinal attachment, while an inspection is recommended after 23 years for the cover plate detail.

Keywords: Fatigue life, Reliability, Road bridge

1. Introduction

Fatigue life assessment of steel bridges asks for consideration of welded joints; a common assumption in fatigue analysis of welded joints is that the fatigue crack initiation phase is almost absent and that all the fatigue life

*Corresponding author

Email addresses: luca.dangelo@epfl.ch (Luca D'Angelo), alain.nussbaumer@epfl.ch (Alain Nussbaumer)

is taken by the crack propagation phase. Within this hypothesis the linear elastic fracture mechanics (LEFM) shows that the fatigue resistance S-N curve is linear when plotted in the $\log(S\text{-}N)$ plane [1]; S-N curve becomes horizontal at the threshold stress range for crack propagation $\Delta\sigma_{th}$, which is referred as constant amplitude fatigue limit (CAFL). Since under variable amplitude (VA) loads even infrequent CAFL-exceeding stress ranges contribute to reduce the $\Delta\sigma_{th}$ [2], then a modified S-N curve having a reduced slope below the CAFL is conventionally used in combination with linear damage accumulation rule (Miner's rule [3]). It follows that the reliable consideration of extreme loads which lie near the CAFL is of primary importance in the fatigue life assessment of motorway bridge. Weigh-In-Motion (WIM) technology provides a powerful tool to face this problem. Prior to recent years, probabilistic approaches were used to extrapolated short period recorded data to long return periods (i.e. one recorded week extrapolated to 120 years) [4] [5]; however recent improvements in WIM technology allows to use recorded traffic data of one or more years. In this research work WIM measurements are coupled with FE analysis to provide realistic definition of traffic-induced stress ranges at different fatigue critical locations of the Venoge bridge, located on the A1 Swiss motorway between Lausanne and Geneva. The Venoge bridge consists of two identical independent bridges (one for each direction) with a 219 meter length divided in four spans (see Figure 1). Each bridge was constructed in 1961 with two girders and then enlarged in 1995 to four girders (see Figure 2). Due to the slow lane (heavy traffic) location only the enlarged bridge section is considered in this study. The bridge fatigue failure probability at the end of the 100-year design life is computed by solving a reliability problem at two selected fatigue critical locations. The critical locations within the bridge are identified by inspection: 1) the weld attachment between the stiffener and the girder lower flange at the middle of the first span (FAT 56 according to [6], where FAT indicates the fatigue strength in MPa at $2 \cdot 10^6$ cycles); and 2) the cover plate welded attachment at the middle of the first span (FAT 40 according to [6]). The fatigue reliability analysis takes in account both the CAFL exceeding event and the critical damage accumulation event : failure probability and related reliability index at the end of design life are computed by estimating the joint failure probability of these two events. Comparisons with target reliability index values indicated in the Eurocode standards are made.

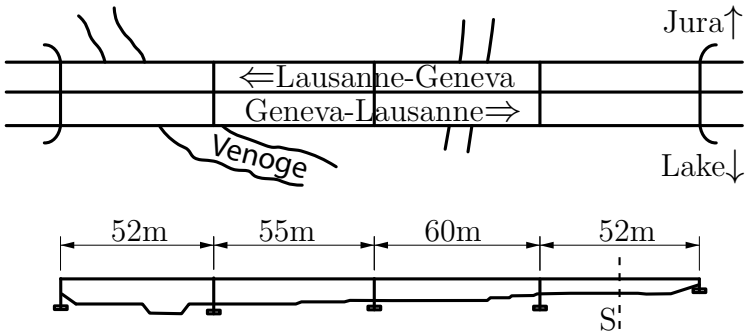

Figure 1: In plane view and elevation

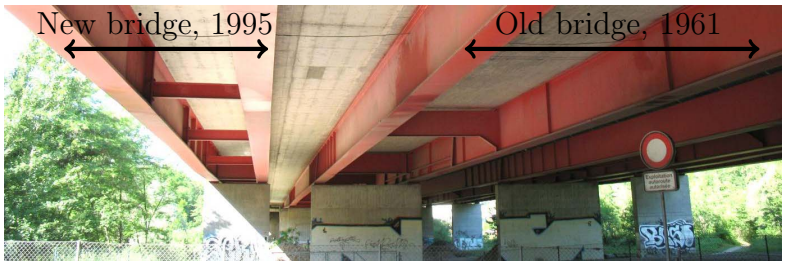

Figure 2: The original bridge and the enlarged section

Year	Vehicles	Axles
2006	$3.863 \cdot 10^5$	$1.391 \cdot 10^6$
2007	$4.045 \cdot 10^5$	$1.448 \cdot 10^6$
2008	$3.988 \cdot 10^5$	$1.439 \cdot 10^6$
Total	$1.190 \cdot 10^5$	$4.278 \cdot 10^6$

Table 1: Observed heavy vehicles

Type	2006	2007	2008	2013
2 Axles	27.4%	27.5%	26.4%	22.1%
3 Axles	9.4%	10.7%	11.0%	11.8%
4 Axles	35.8%	34.2%	34.1%	34.0%
5 Axles	19.3%	20.2%	21.3%	24.9%
6 Axles	1.1%	0.8%	0.7%	0.4%
N.C.[a]	7.0%	6.6%	6.5%	6.9%

Table 2: Heavy traffic composition

[a]N.C.= not classified

2. Traffic analysis

WIM recorded data of the Denges station (1km far from the bridge) for a 3 year period (1.01.2006 - 31.12.2008) were considered in order to get the time-history of bridge crossing vehicles. Direction Lausanne-Geneva was analysed due to the unavailability of complete data for the opposite direction. WIM devices can capture static vehicle axle weights, which allow for characterization of traffic demand in terms of: time of passage (T), vehicle speed (V), number of axles (N), total length (TL), gross total weight (GTW),axles weight (AW), and axles distances (AD). A Matlab code which reads recorded WIM data, classifies vehicles according to GR03-EUR13 classification [7] and produces the 3-year history of bridge crossing axles was developed. Only heavy vehicles with GTW higher than 10 tons were involved in fatigue calculation because lighter vehicles give a negligible contribution to the bridge fatigue damage [8]. Tables 1 and 2 show that there is no significant evolution of traffic during the observed period both in terms of number of observed heavy vehicles and in terms of heavy traffic composition. In order to validate this hypothesis, WIM recorded data from the year 2013[1] were analysed and compared to data from the period 2006-2008. Table 2 and Figure 3 show negligible evolution of traffic from 2006 to 2013 in terms of respectively composition and monthly observations. The 3 year time-history of bridge crossing axles, which has been used for fatigue analysis, is plotted in Figure 4.

[1]Complete data available from 1.03.2013 to 31.12.2013 since in first two months WIM devices did not work continuously

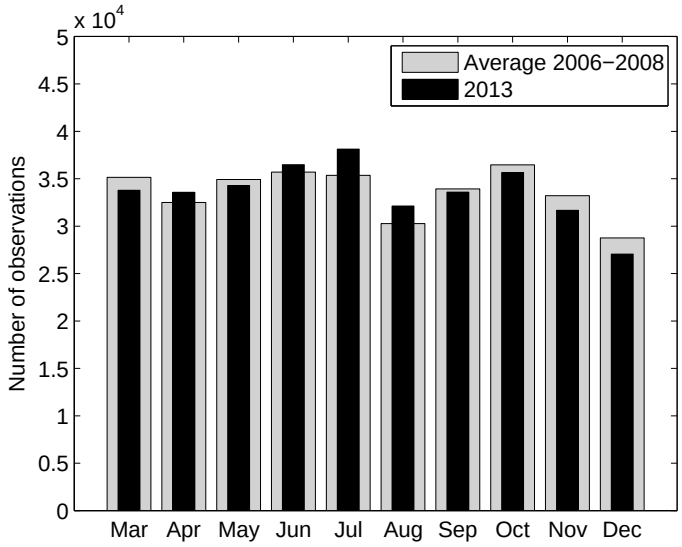

Figure 3: Monthly observations of heavy vehicles

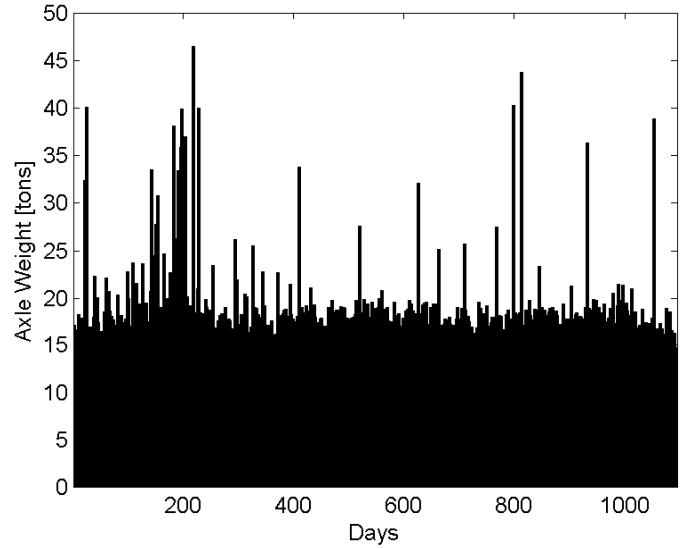

Figure 4: Time history of crossing axles (may include double and triple axles)

3. Reliability framework

In this section the framework for the fatigue reliability analysis of the Venoge bridge is defined. Due to the randomness of traffic loading and fatigue resistance, a probabilistic model has to be established. Two critical fatigue sensitive details have been selected by inspection: 1) the weld attachment between the stiffener and the girder lower flange at the middle of the first span (FAT 56 according to Eurocode standards [6]); and 2) the cover plate welded attachment at the middle of the first span (FAT 40 according to [6]). Since welded details are subjected to VA traffic-induced loadings, fatigue life assessment is done by using linear damage accumulation rule (Miner's rule [3]):

$$D_t = \frac{1}{\exp(C)} \sum_i n_i \Delta\sigma_i^{-m1} + \frac{1}{\exp(C)\exp(V)^{(m_1-m_2)}} \sum_j n_j \Delta\sigma_j^{-m_2} \qquad (1)$$

where:

- D_t is the total accumulated damage
- $\exp(V)$ is the CAFL, which is equal to $0.74FAT$ according to Eurocode standards [6];
- n_i is the i-cycle of the loading spectrum, which has nominal stress range $\Delta\sigma_i$ above the fatigue limit γ;
- n_j is the j-cycle of the loading spectrum, which has the nominal stress range $\Delta\sigma_j$ below the fatigue limit γ;
- m_1 is the slope of the S-N curve for a nominal stress range above the fatigue limit and it is equal to -3 according to Eurocode standards [6];
- m_2 is the slope of the S-N curve for a nominal stress range below the fatigue limit and it is equal to -5 according to Eurocode standards [6]; it allows to take in account the gradual exceedance of the propagation threshold by lower stress range as the crack length increases;
- C is the log-intercept of S-N curve having slope equal to m_1 and it is a random variable, whose parameters are recommended in Tab. C1.10 of [9];

The validity of Eq. 1 is conditioned to the fact that there is at least one cycle of the loading spectrum which exceeds the CAFL:

$$\Delta\sigma_{max} \geq CAFL \tag{2}$$

where $\Delta\sigma_{max}$ is the maximum stress range of the loading spectrum.
Therefore the assessment of the fatigue failure probability of considered critical details asks for consideration of two events:

- E_1: Critical damage accumulation
- E_2: CAFL exceeding

To have fatigue failure, both events E_1 and E_2 must happen. From the definition of conditional probability:

$$P_f = P(E_1 \cap E_2) = P(E_1|E_2)P(E_2) = P(E_1^*)P(E_2) \tag{3}$$

where $E_1^* = E_1|E_2$ represents critical damage accumulation conditioned to CAFL exceeding; definition of limit state equations related to E_1^* and E_2 is discussed in Section 3.1.

3.1. Definition of limit state equations

The limit state equation related to the conditioned event E_1^* is defined as follows:

$$g_1(\underline{x}_1) = d_t - \frac{1}{\exp(c)} \sum_i n_i \Delta\sigma_i^{-m1} - \frac{1}{\exp(c)\exp(v)^{(m_1-m_2)}} \sum_j n_j \Delta\sigma_j^{-m_2} = d_t - \frac{s_d}{\exp(c)} \tag{4}$$

where d_t is a realization of the random variable D_t (critical value of the accumulated damage giving failure, =LogNormal(0,0.3) [10]), s_d is a realization of the random variable S_d (sum of m-power stress ranges over the 100 year design life) and c is a realization of C (see section 3.1.1). Definition of random variables C and S_d are discussed respectively in Section 3.1.1 and 3.1.2.
The failure event E_1^* may be described in the following way:

$$E_1^* = \{g(\underline{x}_1) \leq 0\} \tag{5}$$

where $\underline{x}_1 = (d_t, s_d, c)$.
Having defined the failure event E_1^*, the probability of failure $P(E_1^*) = P(E_1 \cap E_2)/P(E_2)$ may be defined as follows:

$$P(E_1^*) = \int_{g(\underline{x}_1)\leq 0} f_{\underline{X}_1}(\underline{x}_1) d\underline{x}_1 \tag{6}$$

where $f_{\underline{X}_1}(\underline{x}_1)$ is the probability density function (pdf) of $\underline{x}_1$. The related reliability index is:

$$\beta_1 = -\Phi^{-1}(P(E_1^*)) \tag{7}$$

Since the limit state function $g1(\underline{x}_1)$ is not linear, the reliability problem is solved using FORM with Hasofer-Lind approach [11].
The limit state equation related to the event E_2 is defined as follows:

$$g_2(\underline{x}_2) = z_p - exp(v) \tag{8}$$

where z_p is the $\Delta\sigma_{max}$ return level for the return period $\frac{1}{p}$ and v is a realization of random variable $V = \ln(CAFL)$.
According to [9]:

$$V = \begin{cases} Normal(3.59, 0.10) & \text{for } (FAT40) \\ Normal(3.94, 0.11) & \text{for } (FAT56) \end{cases} \tag{9}$$

The definition of return level z_p is discussed in Section 3.1.2.
In analogy with β_1 the reliability index is:

$$\beta_2 = -\Phi^{-1}(P(E_2)) = \int_{g(\underline{x}_2)\leq 0} f_{\underline{X}_2}(\underline{x}_2) d\underline{x}_2 \tag{10}$$

where $f_{\underline{X}_2}(\underline{x}_2)$ is the pdf of $\underline{x}_2$. The reliability problem is solved again using FORM with Hasofer-Lind approach [11].

3.1.1. Resistance model

In this paper fatigue strength S-N curves from Eurocode standards [6] are used. The CAFL is equal to 29.6 MPa for FAT40 detail and 41.4 MPa for FAT56 detail (see Figure 5). The slope of the S-N curve above the CAFL, m_1, is equal to -3 while the slope of the S-N curve below the CAFL, m_2, is equal to -5. The natural logarithm of the intercept of S-N curve having slope m_1, C, is a normal random variable; according to recommendations given in Tab. C1.10 of [9]:

$$C = \begin{cases} Normal(26.18, 0.37) & \text{for } (FAT40) \\ Normal(27.25, 0.41) & \text{for } (FAT56) \end{cases} \tag{11}$$

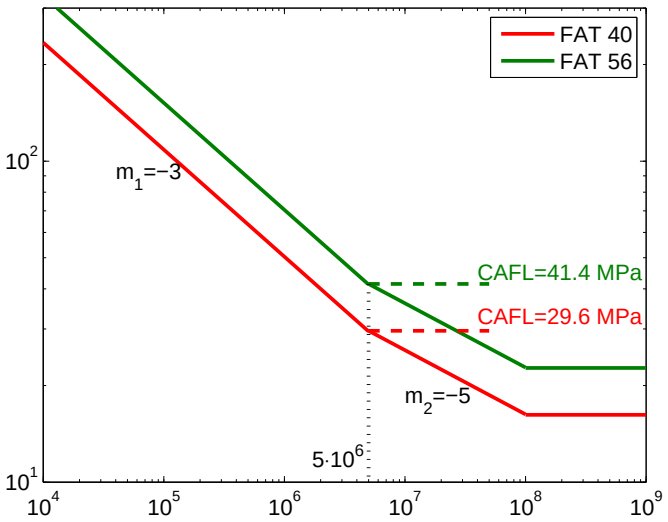

Figure 5: Fatigue strength S-N curves [6]

3.1.2. Loading model

Three-year real traffic-induced time stress history of axle loads was generated using WIM measurements as described in Section 2 (see Figure 4). Stress response influence lines at fatigue critical details were characterized with a refined three-dimensional (3-D) FE model that takes into account the effective transverse load repartition, the cracking of the concrete slab and the elastic stiffness of stud connectors; the FE model was calibrated and validated using experimental load-*vs*-strain results from bridge static tests [12]. MSC/Nastran [13] was used for the analysis. The $\Delta\sigma$ influence line (see Figure 6) of the nominal stress range in the lower flange of critical section (at first midspan) and the loading axles time history were used to compute the three-year $\Delta\sigma$ time history for both critical details.

Return levels of maximum stress ranges

The three-year $\Delta\sigma$ time history for both critical details was divided in 156 weekly blocks. From each block the $\Delta\sigma$ spectrum was computed using a rainflow algorithm and maximum stress range $\Delta\sigma_{max,k}$ (for k=1:156) was extracted (see Figure 7). Within the assumptions that 1) the sequence of observed stress ranges in each block is a sequence of independent ran-

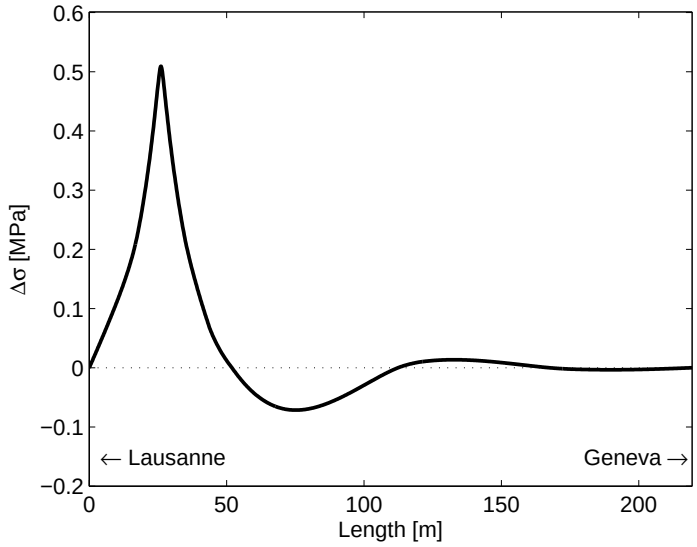

Figure 6: Influence line for nominal $\Delta\sigma$ at first midspan for 1 ton crossing axle

dom variables (or with limited long-range dependance) which have common distribution function; and 2) the pattern of variation of max stress ranges has stayed constant over the observation period (it seems a reasonable assumption from Figure 7), the $\Delta\sigma_{max,k}$ data can be modeled as independent observations from the Generalized Extreme Value (GEV) distribution family. The distribution function of the GEV distribution family is:

$$G(z) = exp\left\{-\left[1+\xi\left(\frac{z-\mu}{\sigma}\right)\right]^{\frac{-1}{\xi}}\right\} = Pr\{\Delta\sigma_{max} \leq z\} \qquad (12)$$

which is defined on $z : 1+\xi\frac{(z-u)}{\sigma} > 0$, with $-\infty < \mu < +\infty$,$\sigma > 0$ and $- < \xi < +\infty$.
Estimated of extreme quantiles of the weekly maximum stress range distribution are obtained by inverting Equation 12:

$$z_p = \begin{cases} \mu - \frac{\sigma}{\xi}[1-\{-\ln(1-p)\}^{-\xi}] & \text{for } \xi \neq 0 \\ \mu - \sigma\ln\{-\ln(1-p)\} & \text{for } \xi = 0 \end{cases} \qquad (13)$$

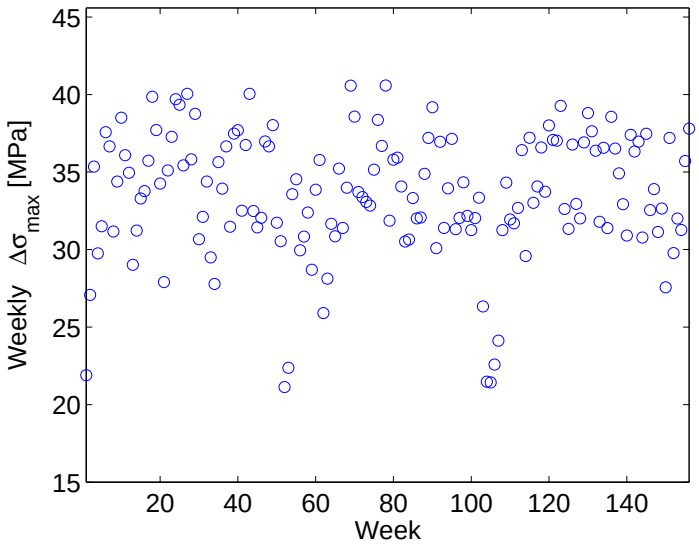

Figure 7: Observed weekly maximum stress ranges during the 3-year observation period

z_p represents the $-p$ return level, which represents the stress range that is exceeded each week with probability p, or alternatively one time every $\frac{1}{p}$ weeks. The parameters of the GEV family distribution (μ, σ, ξ) can be estimated by maximizing the sample log-likelihood, which is:

$$l(\mu,\sigma,\xi) = -156\cdot\ln\sigma - \left(1+\frac{1}{\xi}\right)\sum_{k=1}^{156}\ln\left[1+\xi\left(\frac{\Delta\sigma_{max,k}-\mu}{\sigma}\right)\right] - \sum_{k=1}^{156}\ln\left[1+\xi\left(\frac{\Delta\sigma_{max,k}-\mu}{\sigma}\right)\right]^{\frac{-1}{\xi}} \tag{14}$$

for $\xi \neq 0$, provided that $1+\xi\left(\frac{\Delta\sigma_{max,k}-\mu}{\sigma}\right) > 0$ for $k = 1\ldots156$.
When $\xi = 0$, the log-likelihood is:

$$l(\mu,\sigma,\xi) = -156\cdot\ln\sigma - \sum_{k=1}^{156}\frac{\Delta\sigma_{max,k}-\mu}{\sigma} - \sum_{k=1}^{156}\exp\left\{\frac{\Delta\sigma_{max,k}-\mu}{\sigma}\right\} \tag{15}$$

The maximization of Equation 14 or Equation 15 with respect to model parameters (μ, σ, ξ) leads to the maximum likelihood estimates $(\hat{\mu}, \hat{\sigma}, \hat{\xi})$. It is common to assume that the approximate distribution of $(\hat{\mu}, \hat{\sigma}, \hat{\xi})$ is multivariate normal with mean (μ, σ, ξ) and variance-covariance matrix equal to

the inverse of the observed Fisher information matrix evaluated at maximum likelihood estimates ($I(\hat{\theta}) = \frac{-\delta^2}{\delta\theta_i \delta\theta_j} l(\hat{\theta})$).

By substituting $(\hat{\mu}, \hat{\sigma}, \hat{\xi})$ in Equation 13 the ML estimate of the $\frac{1}{p}$ return level is:

$$\hat{z}_p = \begin{cases} \mu - \frac{\hat{\sigma}}{\hat{\xi}}[1 - \{-\ln(1-p)\}^{-\hat{\xi}}] & \text{for } \xi \neq 0 \\ \hat{\mu} - \hat{\sigma}\ln\{-\ln(1-p)\} & \text{for } \xi = 0 \end{cases} \tag{16}$$

Under the assumption of approximate normality of ML estimators, the Δ method [14] provides the variance-covariance matrix for $\hat{z}_p$:

$$Var(\hat{z}_p) = \nabla z_p^T \underline{\underline{\sum}} \nabla z_p \tag{17}$$

Where $\underline{\underline{\sum}}$ is the variance-covariance matrix of $(\hat{\mu}, \hat{\sigma}, \hat{\xi})$ and

$$\nabla z_p^T = \left[\frac{\delta z_p}{\delta\mu}, \frac{\delta z_p}{\delta\sigma}, \frac{\delta z_p}{\delta\xi}\right] \tag{18}$$

evaluated at $(\hat{\mu}, \hat{\sigma}, \hat{\xi})$.

Sum of m-power stress ranges

The three-year $\Delta\sigma$ time history for both critical details was divided in 156 weekly blocks. From each block the $\Delta\sigma$ spectrum was computed using a rainflow algorithm; then the weekly sum of m-power stress ranges was computed:

$$s_{wk} = \sum_{i=1}^{N_1} n_i(\Delta\sigma_i)^{-m_1} + \frac{1}{(0.74FAT)^{m_1-m_2}} \sum_{j=1}^{N_2} n_j(\Delta\sigma_j)^{-m_2} \qquad \text{for } (k = 1 \cdots 156) \tag{19}$$

Within the assumption that the weekly sum of m-power stress ranges is a normal random variable with location parameter μ_{S_w} and scale parameter σ_{S_w}, the observed sample s_{wk} can was used to make inference about distribution parameters. Under the assumption of no-traffic growth, the sum of m-power stress ranges over the 100 year design life is:

$$S_d = \sum_{i=1}^{100\cdot 52} S_{wi} \tag{20}$$

Location parameter μ_{S_d} and scale parameter σ_{S_d} were computed by making use of the central limit theorem [15].

4. Results

4.1. Event E_1^**: Critical damage accumulation*

Observed weekly sum of m-power stress ranges and fitted normal distribution for two considered details are plotted in Figures 8 and 9. Parameters of the fitted normal distribution S_w are $(\hat{\mu}_{S_w}, \hat{\sigma}_{S_w}) = (3.08 \cdot 10^7, 7.65 \cdot 10^6)$. Parameters of normal distribution S_d over the design life are:

$$(\hat{\mu}_{S_d}, \hat{\sigma}_{S_d}) = \begin{cases} (2.82 \cdot 10^6 \cdot 52N_y, 6.90 \cdot 10^5 \cdot \sqrt{52N_y}) & \text{for } (FAT40) \\ (1.50 \cdot 10^6 \cdot 52N_y, 3.78 \cdot 10^5 \cdot \sqrt{52N_y}) & \text{for } (FAT56) \end{cases} \tag{21}$$

for $N_y = 1 \ldots 100$ (number of years).
The probability and quantile plots for assessing the accuracy of the GEV model fitted to the observed data are given in Figures 10 to 13.
The limit state function g_1 (see Equation4) is completely defined with to Equations 11 and 21; the resolution of the reliability problem defined in Equation 6 gives the evolution of the reliability index $\beta_1 = -\Phi^{-1}(P(E_1^*))$ over the bridge design life. It is recalled here that $P(E_1^*)$ represents the probability of having critical damage accumulation (E_1) given that CAFL has been exceeded (E_2).

4.2. Event E_2*: CAFL exceeding*

Fit of GEV distributions family to observed $\Delta\sigma_{max}$ leads to the ML estimate:

$$(\hat{\mu}, \hat{\sigma}, \hat{\xi}) = (35.593, 4.351, -0.518) \tag{22}$$

The probability and quantile plots for assessing the accuracy of the GEV model fitted to the observed data are shown in Figures 14 and 15. The approximate variance covariance matrix of the parameter estimates is:

$$\underline{\underline{\Sigma}} = \begin{pmatrix} 0.0020 & -0.0082 & -0.0060 \\ -0.0082 & 0.0785 & -0.0353 \\ -0.0060 & -0.0353 & 0.1400 \end{pmatrix} \tag{23}$$

ML estimates of $\Delta\sigma_{max}$ return levels,$\hat{z}_p$, are computed by substituting ML estimate of GEV distribution parameters vector into Equation 16 ; Figure 16 represents $\hat{z}_p$ against observed values (empirical return levels).
Variance matrix $\underline{\underline{\Sigma}}$ allows to compute confidence intervals for return levels z_p, using Delta method (see Equation 16); 95% confidence intervals of return

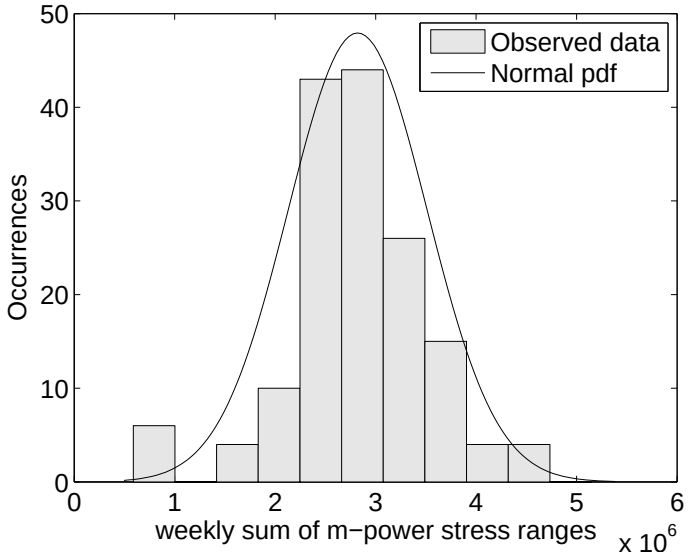

Figure 8: Fitting of observed m-power stress ranges (FAT40)

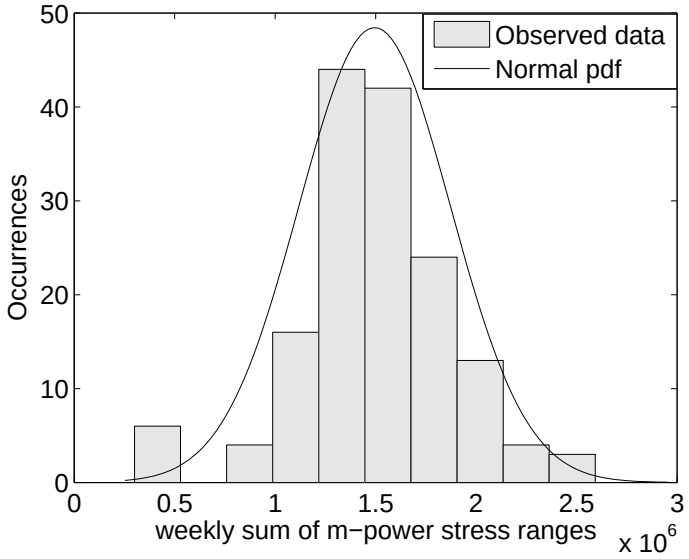

Figure 9: Fitting of observed m-power stress ranges (FAT56)

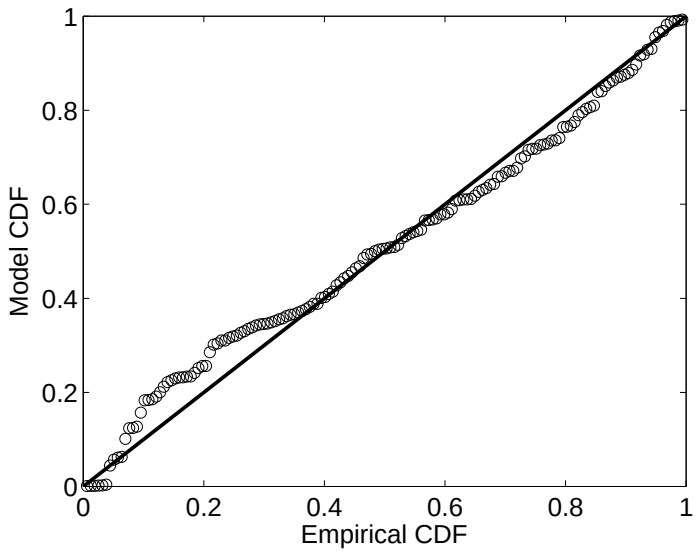

Figure 10: Probability plot for the Normal fit to observed m-power stress ranges (FAT40)

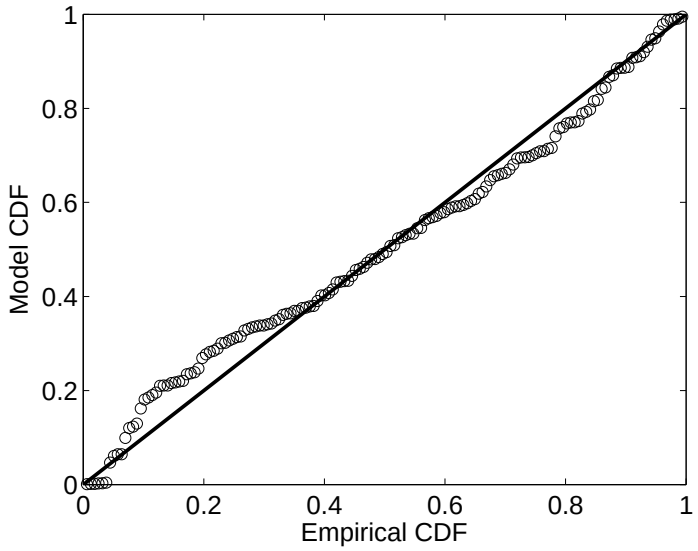

Figure 11: Probability plot for the Normal fit to observed m-power stress ranges (FAT56)

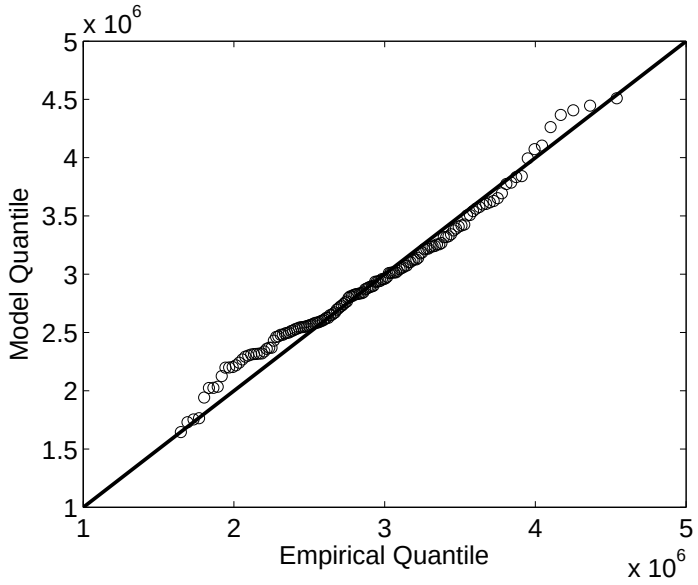

Figure 12: Quantile plot for the Normal fit to observed m-power stress ranges (FAT40)

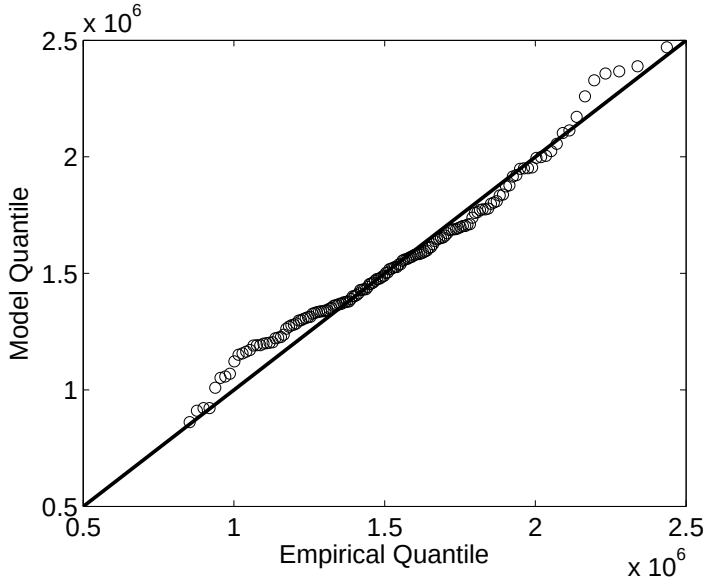

Figure 13: Quantile plot for the Normal fit to observed m-power stress ranges (FAT56)

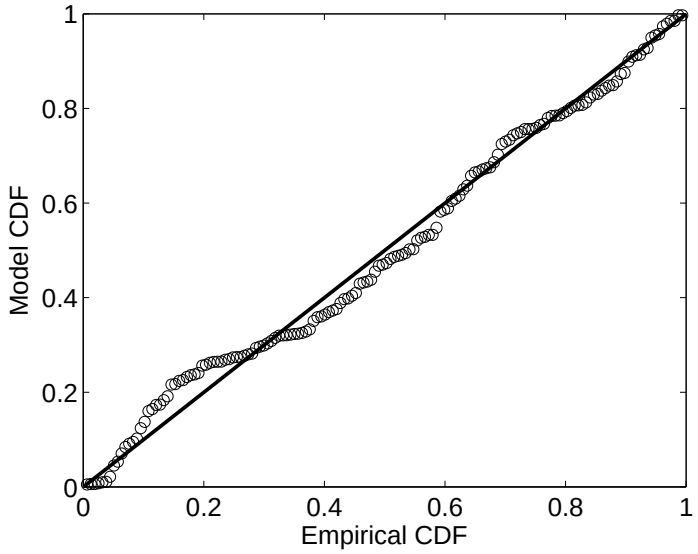

Figure 14: Probability plot for the GEV fit to observed $\Delta\sigma_{max}$

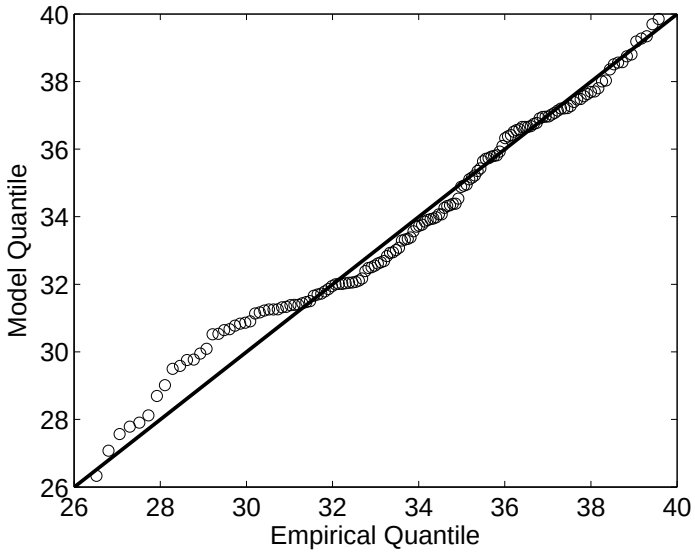

Figure 15: Quantile plot for the GEV fit to observed $\Delta\sigma_{max}$

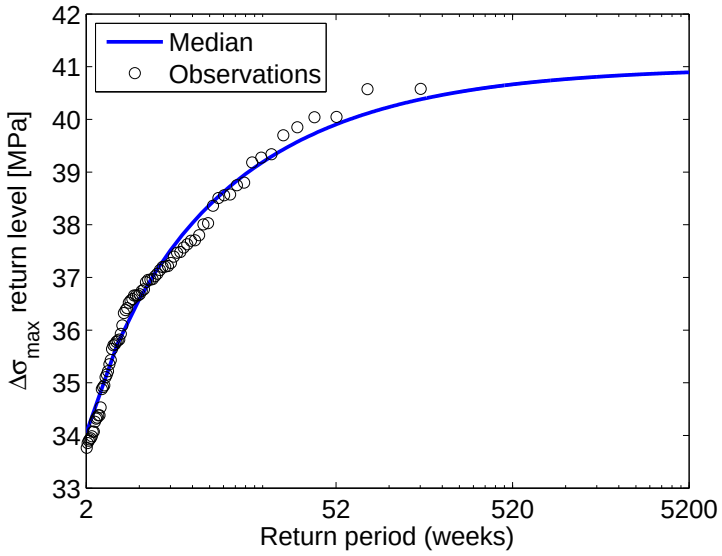

Figure 16: Return level plot: fit to observed data

levels of return levels z_p are shown in Figure 17.
The limit state function g_2 (see Equation 8) is completely defined with Equations 9,22 and 23; the resolution of the reliability problem defined in Equation 10 gives the evolution of the reliability index $\beta_2 = -\Phi^{-1}(P(E_2))$ over the bridge design life. It is recalled here that $P(E_2)$ represents the probability of CAFL exceedance.

4.3. Combined analysis: detail fatigue failure

According to Equation 3, the probability of fatigue failure is given by the product of probabilities $P(E_1^*)$ and $P(E_2)$; the fatigue reliability index $\beta = -\Phi^{-1}(P(E_1^* \cdot E_2))$ has been computed using results of Sections 4.1 and 4.2. The evolution of the fatigue reliability index β over the 100 year design life is shown in Figure 18. Following reliability indexes are also plotted in Figure 18 for direct comparison:

- $\beta_{target}^{\text{EN1990}}$, based on an annual failure probability equal to $1.3 \cdot 10^{-}6$ (Reliability class RC2, assuming independency, [16] Annex C, Chapter C6)
- $\beta_{target}^{\text{JCSS}}$, based on an annual failure probability equal to $1.3 \cdot 10^{-}5$ (Normal

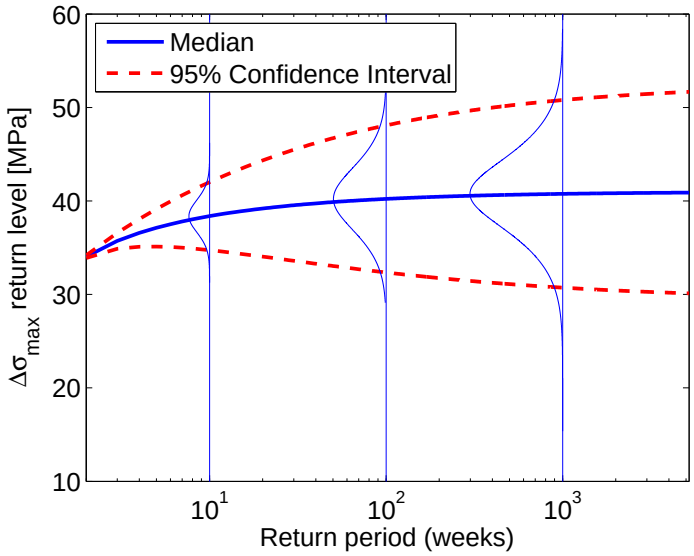

Figure 17: Return level plot: median and 95% confidence interval

relative cost of safety measure and moderate consequence of failure, assuming independency [17])

In order to check the accuracy of the FORM approach, the reliability index β for the $FAT40$ detail was computed after 18 and 100 years,using SORM approach. The reliability indexes based on FORM and SORM approaches are compared in Table 3.

5. Discussion

In this study the fatigue failure probability, P_f, of two critical details (classified as $FAT40$ and $FAT56$ [6]) and related reliability index, β, were computed for a 100 year-design life. Failure probability P_f was computed as product of $P(E_2)$ (probability of CAFL exceeding) and $P(E_1|E_2) = P(E_1^*)$ (probability of having critical damage accumulation conditioned to CAFL exceeding).
Assessment of $P(E_1|E_2)$ and $P(E_2)$ asks respectively for definition of limit state equations g_1 (see Equation 4) and g_2 (see Equation 8).
Concerning the limit state function g_1, the random variables C and D_t, which represent resistance terms of function, were defined according to [10] and [6].

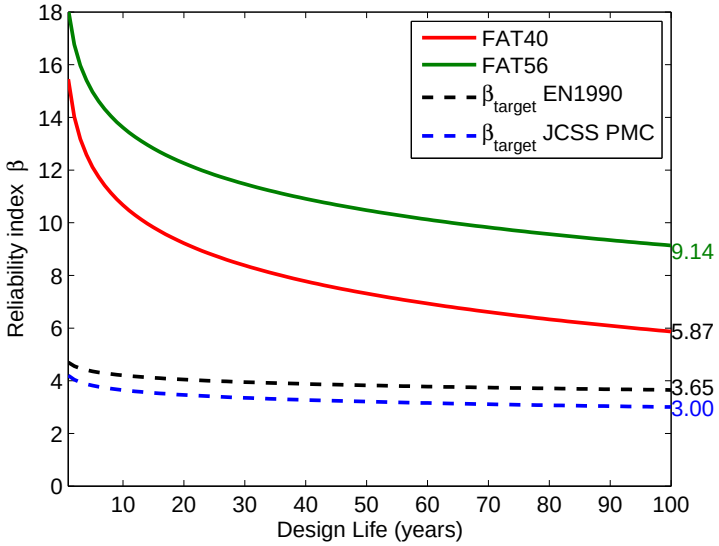

Figure 18: Evolution of reliability index β over the design life

The random variable S_d , representing the loading term of limit state equation g_1, was defined by fitting Normal distribution S_w (weekly sum of m-power stress ranges) to 156 weekly observations and then applying central limit theorem in order to switch from S_w parameters to S_d parameters. The accuracy of the Normal fit to observed s_w sample can be assessed by looking at following graphs: 1) the density plot (see Figures 8 and 9); 2) the probability plot (see Figures 10 and 11); and 3) the quantile plot (see Figures 12 and 13).
Diagnostic plots above provide support to the fitted Normal model for both considered details.
Concerning the limit state function g_2, the random variable V, representing the resistance term of the function, was defined according to [9]. The $\Delta\sigma_{max}$ return level ,z_p, representing the loading term of limit state function g_2, was defined by fitting GEV family distribution to 156 weekly max stress ranges and then computing quantiles of fitted distribution. The accuracy of the GEV fit to observed $\Delta\sigma_{max}$ sample can be assessed by looking at following graphs: 1) the probability plot (see Figure 14); 2) the quantile plot (see Figure 15); and 3) the return level plot (see Figure 16).
Diagnostic plots above provide support to the fitted GEV model.

Failure probabilities $P(E_1^*)$ and $P(E_2)$, and related reliability indexes β_1 and β_2 were computed for both considered details using FORM approach. Comparison of FORM-based and SORM-based reliability indexes for the $FAT40$ detail, after 10, 50, and 100 years (see Table 3), shows that the difference in the β value is negligible and there is no need to use SORM approach. Figure 18 shows the evolution of reliability index $\beta = -\Phi^{-1}(\Phi(-\beta_1) \cdot \Phi(-\beta_2))$ over the 100-year design life: for both $FAT40$ and $FAT56$ details the reliability index is greater than $\beta_{target}^{\text{JCSS}}$ and $\beta_{target}^{\text{EN1990}}$ over whole bridge design life.

Number of years	β_{FORM}	β_{SORM}
10	10.67	10.66
50	7.31	7.31
100	5.87	5.86

Table 3: Comparison between FORM and SORM approach, $FAT40$ detail

6. Future work

The fatigue strength characterization of the considered details based on Eurocode standards is affected by lack of accuracy. Indeed the Eurocode approach for the definition of S-N curves from experimental data has several limitations: 1) run-out points are neglected; 2) the CAFL is arbitrarily assumed to begin at 5 million cycles; and 3) characteristic curves are based on fatigue data scatter in finite life region ($N < 10^6 cycles$) resulting in less accuracy in the high cycle fatigue region ($N > 10^6 cycles$). These limitations may lead to inaccurate characterization of random variables C and V. Furthermore the Miner's rule approach has two limitations: 1) the parameters of random variable D_t proposed by Wirsching [10] can not be generally applied to all details (Tables C1 in [1]); and 2) general application of the S-N curve slope below the CAFL, $m_2 = -5$ ([2]), needs experimental validation based on VA fatigue experimental tests.
In order to overcome these limitations, a novel probabilistic approach for estimation of VA S-N curves using experimental results is under development. Random variables V, C, m_1, m_2, and D_t are included in the parameters vector of the stochastic model that relates the applied stress range to the number of cycles to failure.
Fatigue strength characterization of critical details based on novel approach will allow to improve the confidence in the fatigue reliability analysis.

For the considered study case of the Venoge bridge, the influence length of the considered structural elements is higher than 52 m; Brüwilher et al. [18] suggested a load dynamic amplification factor equal to unity for influence lengths longer than 40 m: for the specific case the issue of the load dynamic amplification effect has not been addressed. However, for a generic case, this effect has to be taken in account for the definition of loading spectra.

7. Conclusions

In this paper a framework for the fatigue reliability analysis of a highway bridge has been formulated in terms of the joint probability of two events: the CAFL exceeding and the critical damage accumulation. The framework has been applied to the Venoge bridge, within the A1 Swiss Motorway. Three year-continuous registration WIM data and FE analysis were combined to compute the time-stress response at two different fatigue critical locations. ML technique and extreme value theory have been used to define the parameters of loading terms of limit state functions. Fatigue strength of critical details has been defined according to Eurocode standards. Finally the fatigue failure probability and related reliability index are calculated over the 100 year-bridge design life for both critical details. The results show that fatigue is not a concern for both $FAT40$ and $FAT56$ details, according to EN 1990 and JCSS PMC, which is evident by a reliability index greater than $\beta_{target}^{\text{JCSS}}$ and $\beta_{target}^{\text{EN1990}}$ at the end of the fatigue life.
The reliability analysis framework set up in this paper constitute a powerful tool to perform fatigue reliability analysis of road bridges using WIM-based realistic characterization of traffic loadings. Current analysis uses 2006-2008 WIM data and is based on stationary load sequences; however any additional WIM dataset can be used to update estimated model and to take in account possible future traffic growth (non-stationary loading sequences). Moreover, future advances in better characterization of the fatigue strength curves of critical details, will give a more realistic view on the real reliability index calculation over bridge design life.

8. Acknowledgements

This research was supported by the Swiss Federal Roads Office (FEDRO Project AGB 2010/003).

[1] T. Gurney, Fatigue of welded structures, 2nd Edition, Cambridge University Press, 1979.

[2] F. C. Smith, C. Castiglioni, P. B. Keating, Analysis of fatigue recommendations using new data, IABSE Periodica (3) (1989) 97–109.

[3] M. A. Miner, Cumulative damage in fatigue, Journal of Applied Mechanics 12 (1945) 159–164.

[4] S. F. Bailey, Basic principles and load models for the structural safety evaluation of existing road bridges, Ph.D. thesis, Ecole Polytechnique Fédérale de Lausanne (1996).

[5] C. Crespo-Minguillón, J. Casas, A comprehensive traffic load model for bridge safety checking, Structural Safety 19 (4) (1997) 339–359.

[6] European Committee for Standardization, Eurocode 3: Design of steel structures - Part 1-9: Fatigue (2005).

[7] T. Meystre, M. A. Hirt, Evaluation de ponts routiers existants avec un modèle de charge de trafic actualisé, Mandat de recherche AGB 2002/005 (2006).

[8] C. G. Schilling, Variable amplitude load fatigue, Task A - Literature Review. Volume I. Traffic loading and bridge response. Interim report (1990).

[9] Technical European Convention for Constructional Steelwork - TC6, Recommendations for the fatigue design of steel structures (1985).

[10] B. P. H. Wirsching, M. Asce, Fatigue reliability for offshore structures, Journal of Structural Engineering 110 (10) (1985) 2340–2356.

[11] A. M. Hasofer, N. C. Lind, An exact and invariant first order reliability format, Journal of the Engineering Mechanics Division ASCE 100 (1974) 111–121.

[12] O. Burdet, Pont sur la Venoge (VD) côté Jura , après la solidarisation, Rapport d'essai de charge statique, Tech. Rep. Vd, EPFL, IBAP, Lausanne (1997).

[13] MSC Software, MSC Nastran Quick Reference Guide (2012).

[14] G. Casella, R. L. Berger, Statistical Inference, 2002.

[15] D. D. Wackerly, W. Mendenhall, R. L. Scheaffer, Mathematical Statistics, with Application, 7th Edition, Thomson.

[16] European Committee for Standardization, Eurocode EN 1990 - Basis of structural design (2001).

[17] Joint Committee Structural Safety, JCSS Probabilistic Model Code: Resistance Models (2013).

[18] E. Brüwhiler, J.-P. Lebet, Updating of traffic loads on existing bridges, in: IABSE (Ed.), Codes in Structural Engineering Developments and Needs for International Practice, Dubrovnik, 2010.